

Analysis of Electromagnetic Vibration and Noise Characteristics of Bearingless Switched Reluctance Motor

Yonghong Huang^{*}, Chi Chen, Ye Yuan, Fengxiao Huang, Qian Wen Xiang, and Fan Yang

Abstract—The vibration and noise problems caused by the radial electromagnetic force of the Bearingless Switched Reluctance Motor (BSRM) severely restrict its wide application. The purpose of this paper is to research the electromagnetic vibration and noise of Single-Winding Bearingless Switched Reluctance Machine (SWBSRM). Firstly, the radial electromagnetic force, which is the excitation source of electromagnetic vibration, is analyzed. Secondly, the three-dimensional (3D) model of stator structure is established by ANSYS finite element analysis (FEA) software, and its modal analysis is carried out to obtain its modal shape and corresponding modal frequency, which provides a reference and basis for researching the mechanical vibration of the SWBSRM. Finally, the harmonic response field analysis and sound field analysis model are established, and the vibration and noise of the motor under radial electromagnetic force are analyzed by using the magnetic-solid weak coupling analysis method.

1. INTRODUCTION

Switched Reluctance Motor (SRM) is a doubly salient motor with a simple structure and no winding on the rotor, which has many advantages such as high temperature resistance, flexible control mode, and large mechanical strength. It is suitable for high-speed operation under harsh conditions such as high temperature and aerospace [1]. However, the serious vibration and noise problems caused by its inherent mechanical wear limit its application in a wider field.

Bearingless Switched Reluctance Motor (BSRM) superimposes suspension windings on the stator windings of the original SRM. By reasonable control, it generates both suspension force and electromagnetic torque to realize the suspension and rotation of the motor rotor. On the basis of inheriting the excellent characteristics of SRM, BSRM solves the problems of wear and lubrication caused by mechanical bearings [2], which has a more extensive application prospect in flywheel batteries [3], aerospace, and high-speed machine tools.

However, BSRM as a special SRM improves the vibration and noise of SRM to a certain extent, but it also has a double salient structure and a switching power supply, the suspension force and torque, which are still provided by electromagnetic force. Researches show that the pulsating radial electromagnetic force is the source of the vibration in SRM [4, 5], and when the harmonic frequency of the radial electromagnetic force is consistent with the natural frequency of the stator, resonance causing serious noise problems will occur. Therefore, analyzing the BSRM electromagnetic force plays an important role in studying the electromagnetic vibration and noise of the motor.

In order to solve the problem of vibration and noise, scholars mainly focus on the study of vibration and noise sources of SRM, and a series of optimization schemes and control strategies of its structure [6–8] to help reduce vibration and noise, but there are few studies on vibration and noise of BSRM. Ref. [9] analyzes the radial electromagnetic force of SRM by using finite element model. Ref. [10] analyzes the modal shape and natural frequency of SRM stator structure. Ref. [11] proposes a new fast

Received 13 June 2019, Accepted 26 August 2019, Scheduled 17 September 2019

^{*} Corresponding author: Yonghong Huang (hyh@ujs.edu.cn).

The authors are with the School of Electrical and Information Engineering, Jiangsu University, Zhenjiang 212013, China.

computation method for radial vibration in SRM. Ref. [12] introduces the calculation method of radial force in SRM, and the relationship between radial electromagnetic force and electromagnetic vibration is analyzed to predict the noise level at different frequencies accurately. Ref. [13] proposes a new structure with skewed stator and rotor, which is verified by experiments that the structure can reduce vibration and noise effectively. Ref. [14] analyzes the distribution and influence of radial electromagnetic force and electromagnetic in 6/10 pole SRM. Ref. [15] is based on the characteristics of radial force and vibration theory in BSRM and proposes the mathematical model of radial force suitable for BSRM, which combines Maxwell tensor method and magnetic circuit method. Ref. [16] analyzes the radial force model of BSRM with rotor eccentricity, and the correctness of the model is verified by finite element method.

BSRM is divided into two kinds of topologies: Double-Winding Bearing Less Switched Reluctance Machine (DWBSRM) and Single-Winding Bearing Less Switched Reluctance Machine (SWBSRM) [17–20]. In this paper, a 12/8 pole SWBSRM is taken as the research object to analyze the vibration and noise problem. The transient analysis of SWBSRM electromagnetic field is carried out by 2D finite element model. Then the natural frequency and mode shape of the stator structure are solved by finite element analysis software ANSYS Workbench. Lastly, the magnetic-solid weak coupling analysis method is used to analyze the harmonic response vibration and sound pressure of the stator under the electromagnetic force coupling of ANSYS Workbench simulation platform to research the characteristics of electromagnetic vibration and noise. A general overview of the vibration and noise investigation of SWBSRMs is illustrated in Fig. 1.

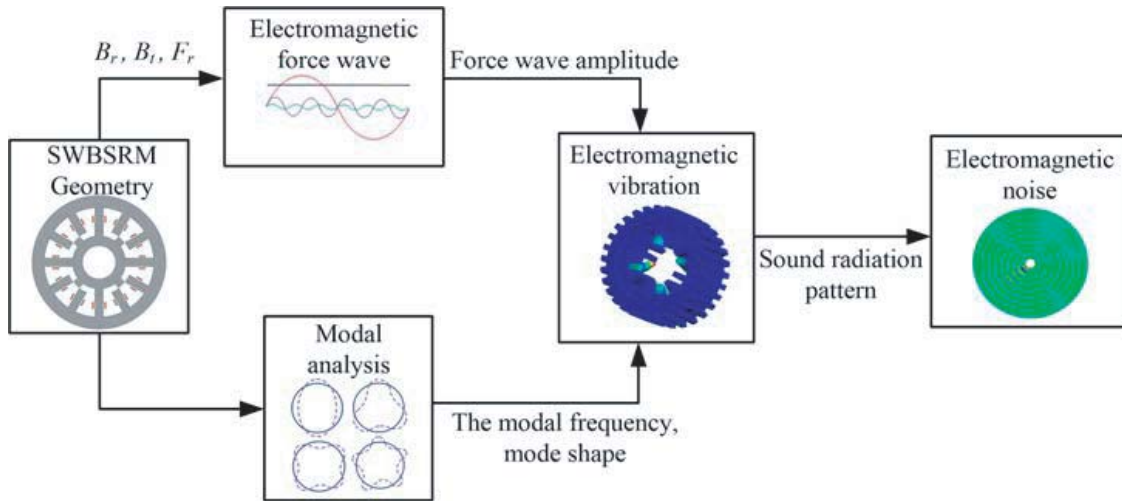


Figure 1. Flowchart for investigating vibration and noise of SWBSRM.

2. SWBSRM ELECTROMAGNETIC FORCE ANALYSIS

2.1. Structure and Operating Principle of SWBSRM

The structure of 12/8 pole SWBSRM is shown in Fig. 2, taking phase A as an example, there is only one winding on each stator tooth pole, and each winding is controlled independently. The current flowing into each pole winding can be equivalent to the torque current component and suspension current component. Among them, the torque current component produces quadrupole torque magnetic field which can not only rotate the rotor but also generate a bias magnetic field, and the suspension current component $i_{sA\alpha}$, $i_{sA\beta}$ produces the suspension magnetic field in the direction of α and β , respectively, and then generating controllable radial suspension force in α and β directions to realize rotor suspension. The suspension principle of phase B and phase C is the same as phase A, and they are placed counterclockwise along phase A windings at 30° and 60° , respectively.

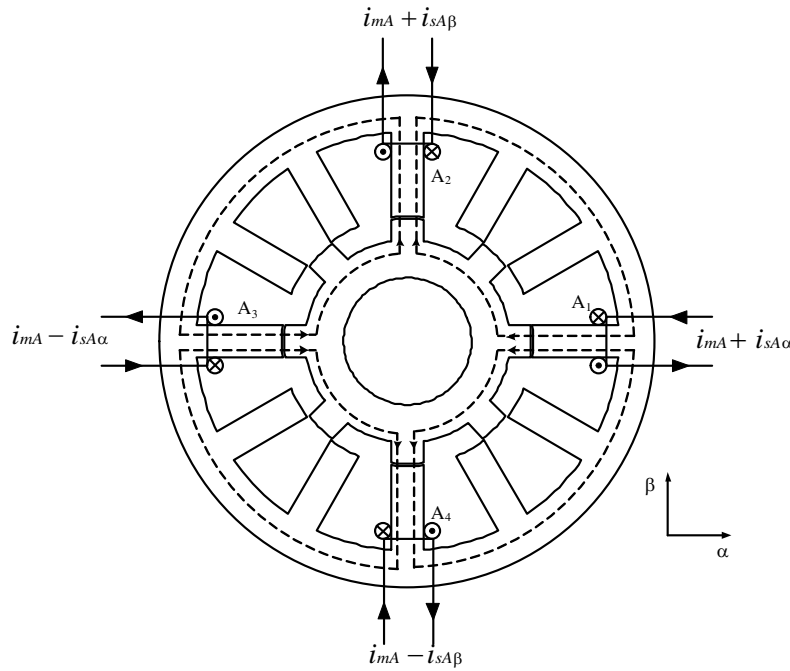


Figure 2. Structure of SWBSRM.

2.2. SWBSRM Radial Electromagnetic Force Analysis

According to different sources of vibration generated by the motor, it can be mainly divided into: electromagnetic vibration, mechanical vibration, and aerodynamic vibration. Since SWBSRM adopts bearingless design and natural cooling mode, electromagnetic vibration is the main vibration source of the motor. Electromagnetic vibration is caused by the electromagnetic force wave generated by the magnetic field in the air gap of the stator and rotor. This force changes not only with time but also with space. Therefore, it can be decomposed into radial component and tangential component. The tangential component causes the bending deformation of the stator and rotor tooth roots of the motor to produce local vibration, which is a secondary cause of electromagnetic vibration. The radial component causes periodic radial deformation of the stator and rotor of the motor, which is a major factor in the generation of electromagnetic vibration. Therefore, analysis of radial electromagnetic force is essential for the subsequent study of electromagnetic vibration and noise.

In this paper, the finite element analysis (FEA) method is used to research the electromagnetic field of SWBSRM. The 2D model of SWBSRM is established by Maxwell software, and the transient analysis of electromagnetic field is carried out to calculate air gap magnetic density and radial electromagnetic force. Its main parameters of three-phase 12/8 pole SWBSRM are shown in Table 1.

According to the Maxwell stress equation, it is necessary to solve the radial and tangential

Table 1. Dimensions of SWBSRM.

Parameter	Value	Parameter	Value
Rated power (W)	2200	Rotor outer diameter (mm)	58
Rated speed (rpm)	10000	Rotor inner diameter (mm)	30
Rated voltage (V)	380	Air gap (mm)	0.5
Stator outer diameter (mm)	121	Axial length (mm)	60
Stator inner diameter (mm)	59	Pole arc (°)	15

components of the air gap magnetic field in order to obtain the radial electromagnetic force and tangential electromagnetic force of the inner surface of the stator, but the radial and tangential components cannot be obtained directly by Maxwell; therefore, the radial components and tangential components need to be solved with the help of Maxwell field calculator. In the finite element simulation, the air gap magnetic field needs to be decomposed into the x -axis component and the y -axis component, and then the radial air gap magnetic density and tangential air gap magnetic density can be obtained according to Equations (1) and (2):

$$B_r = B_x \times \cos(\theta) + B_y \times \sin(\theta) \quad (1)$$

$$B_t = B_y \times \cos(\theta) - B_x \times \sin(\theta) \quad (2)$$

where B_r — radial magnetic density; B_t — tangential magnetic density; B_x — x -axis component of magnetic density; B_y — y -axis component of magnetic density; θ — column coordinate.

The spatial distribution of air gap magnetic density obtained by FEA is shown as follows: Fig. 3 is the radial air gap magnetic density diagram, and Fig. 4 is the tangential air gap magnetic density diagram. It can be seen that the amplitude of tangential air gap magnetic density is small. Therefore, its influence on electromagnetic force wave can be ignored, which verifies that tangential component is the secondary factor of electromagnetic vibration. The maximum amplitude of the radial air gap magnetic density is close to 1 T.

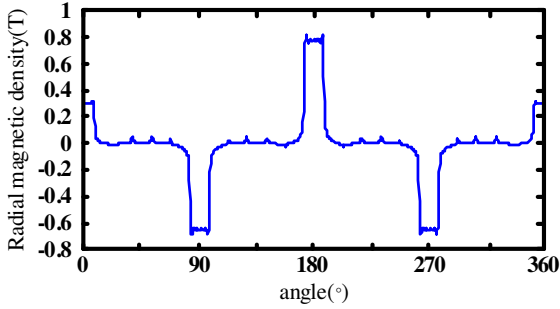


Figure 3. Radial air gap magnetic density diagram.

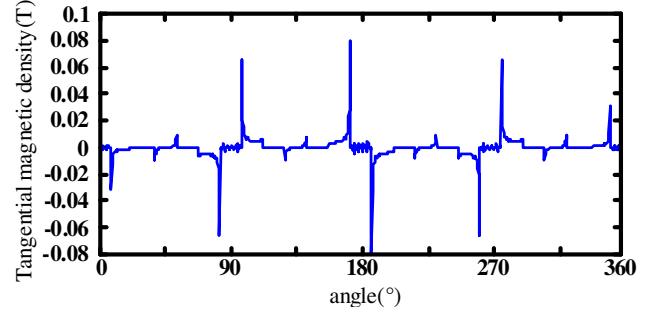


Figure 4. Tangential air gap magnetic density diagram.

Electromagnetic force waves are essentially stresses, and the unit is N/m^2 . According to Maxwell stress tensor method, the radial electromagnetic force density per unit area of stator core can be expressed as follows:

$$F_r = \frac{B_r^2 - B_t^2}{2 \times \mu_0} \quad (3)$$

where μ_0 — vacuum permeability; F_r — radial electromagnetic force density; F_r is related to radial and tangential components of magnetic induction intensity and vacuum permeability.

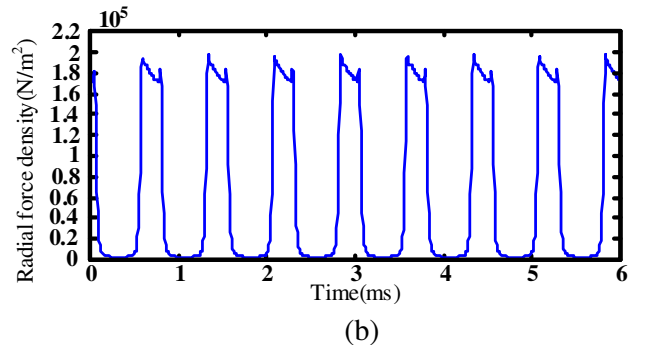
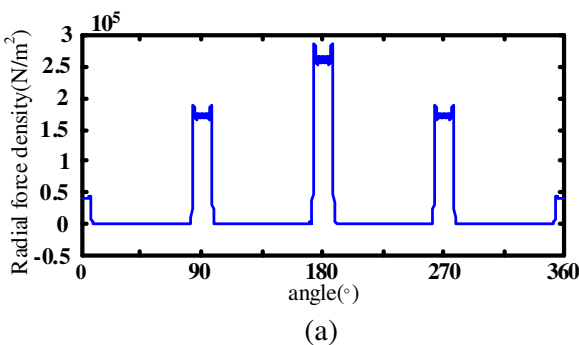


Figure 5. Radial electromagnetic force density distribution diagram. (a) Spatial, (b) temporal.

The density of radial electromagnetic force is obtained by FEA, shown in the diagram. The spatial distribution of radial electromagnetic force density is shown in Fig. 5(a), and the temporal distribution of radial electromagnetic force density is shown in Fig. 5(b). Fig. 6 is the spatial and temporal 3D distribution of radial electromagnetic force density. Combined with the analysis of Fig. 3, Fig. 5, and Fig. 6, it can be seen that the radial electromagnetic force density is large where the radial air gap magnetic density is large, and the electromagnetic force density changes with time and space simultaneously.

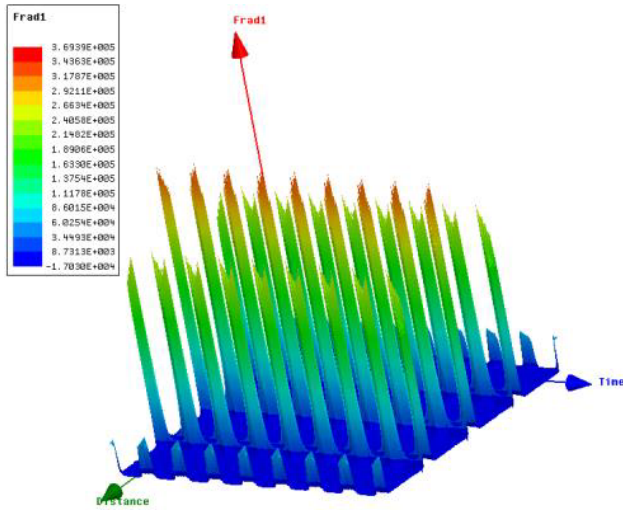


Figure 6. Radial electromagnetic force wave 3D diagram.

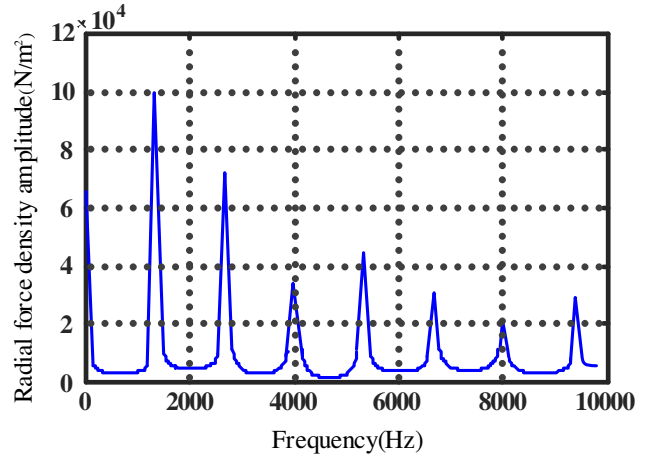


Figure 7. Spectrogram of radial electromagnetic wave.

Figure 7 is a spectrogram of FFT decomposition of time-varying radial electromagnetic force density. From the simulation results, the peak moments of the electromagnetic force waves are 0 Hz, 1333 Hz, 2667 Hz, 4000 Hz, 5334 Hz, 6667 Hz, 8000 Hz, and 9200 Hz.

3. STRUCTURAL MODAL ANALYSIS OF SWBSRM

In order to research the vibration of motor, on the one hand, it is necessary to analyze the excitation source of vibration — radial electromagnetic force. On the other hand, the structural mode of motor should be analyzed. The structural modal analysis of motor mainly includes two important parameters, namely the modal frequency and modal mode. Referring to a large number of references, the methods of modal analysis can be divided into two categories. One is the analytical calculation method, which can get the analytical expression of modal frequency, and this method is fast but has poor accuracy. The other is the energy method, which includes the Fourier series solution and finite element solution. With the rapid development of microcomputer technology, FEA has been widely used due to its high computational accuracy. In this section, the modal analysis of SWBSRM stator structure is carried out by FEA so as to obtain its natural modal frequency and modal shape.

3.1. Mathematical Model of Stator Modal

For the convenience of analysis, the SWBSRM stator is regarded as a multi-degree of freedom system, and its coordinates are expressed as $r_1, r_2, r_3 \dots r_N$. Using the stiffness method, the motion differential equation of the system is established as follows:

$$\sum_{j=1}^N m_{ij} \ddot{r}_j(t) + \sum_{j=1}^N c_{ij} \dot{r}_j(t) + \sum_{j=1}^N k_{ij} r_j(t) = f_i(t), \quad i = 1, 2, 3, \dots, N \quad (4)$$

where m_{ij} — mass coefficient; c_{ij} — damping factor; k_{ij} — stiffness coefficient. The matrix form of Equation (4) can be written as:

$$[M] \{\ddot{R}\} + [C] \{\dot{R}\} + [K] \{R\} = \{F(t)\} \quad (5)$$

where $[M]$ — mass matrix; $[C]$ — damping matrix; $[K]$ — stiffness matrix; $\{\ddot{R}\}$ — acceleration vector; $\{\dot{R}\}$ — speed vector; $\{R\}$ — displacement vector; $F(t)$ — force vector.

Generally, when calculating the natural frequency of the stator, SWBSRM is regarded as undamped vibration. Therefore, in the above Equation (5), the damping is neglected. Let $\{F\} = \{0\}$, and the eigenvalue equation of the undamped modal analysis of the stator is:

$$([K] - \omega^2[M]) \{R\} = \{0\} \quad (6)$$

Making the equation have a non-zero solution, there is:

$$|[K] - \omega^2[M]| = 0 \quad (7)$$

The natural frequencies and modal modes of the SWBSRM stator are obtained by solving ω and $\{R\}$ of Equations (6) and (7).

3.2. Stator Mode Finite Element Analysis

In this paper, ANSYS is used to establish a 3D finite element structure model as shown in Fig. 8. Because the weight of the winding is relatively light, and the junction box and mounting feet have little effect on the free vibration frequency of the stator, the model simplifies the winding, junction box, mounting feet, etc. The material parameter is designed as shown in Table 2.

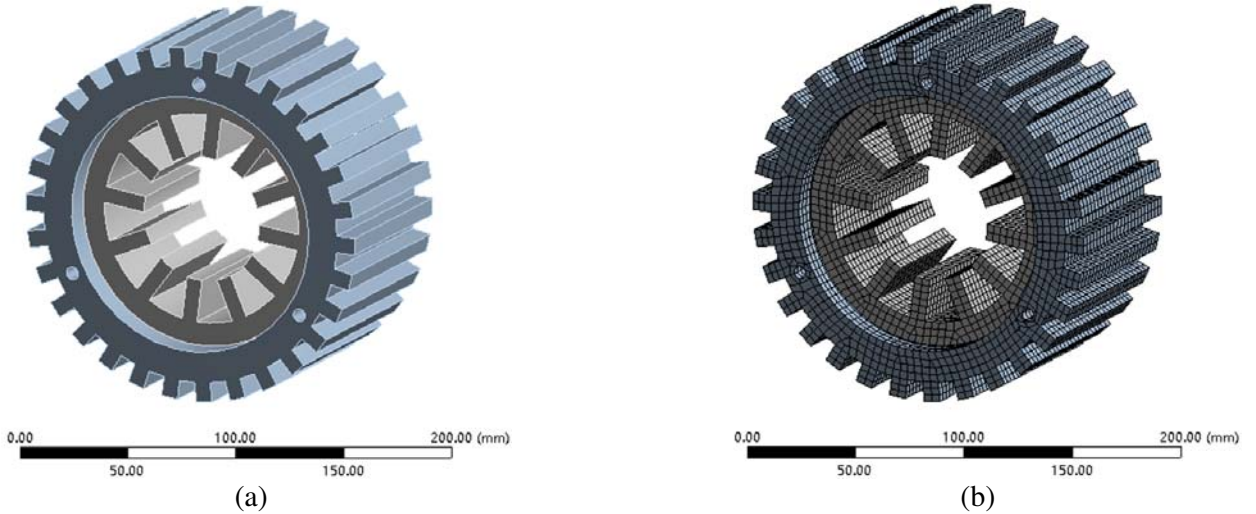


Figure 8. 3D models of SWBSRM stator with shell. (a) Geometry model. (b) Finite-element model.

Table 2. Dimensions of material.

Component	Material	Young's modulus (p_a)	Density (kg/m^3)	Poisson's ratio
Stator core	DW360_50	2.0×10^{11}	7.6×10^3	0.3
Stator shell	Gray cast iron	1.26×10^{11}	7.0×10^3	0.25

After the stator subdivision is completed, the solution is carried out to analyze the dynamic performance of the stator under the free vibration state. The natural frequencies corresponding to the natural modes of the stator can be obtained by setting the 3D extended mode to 50 and the

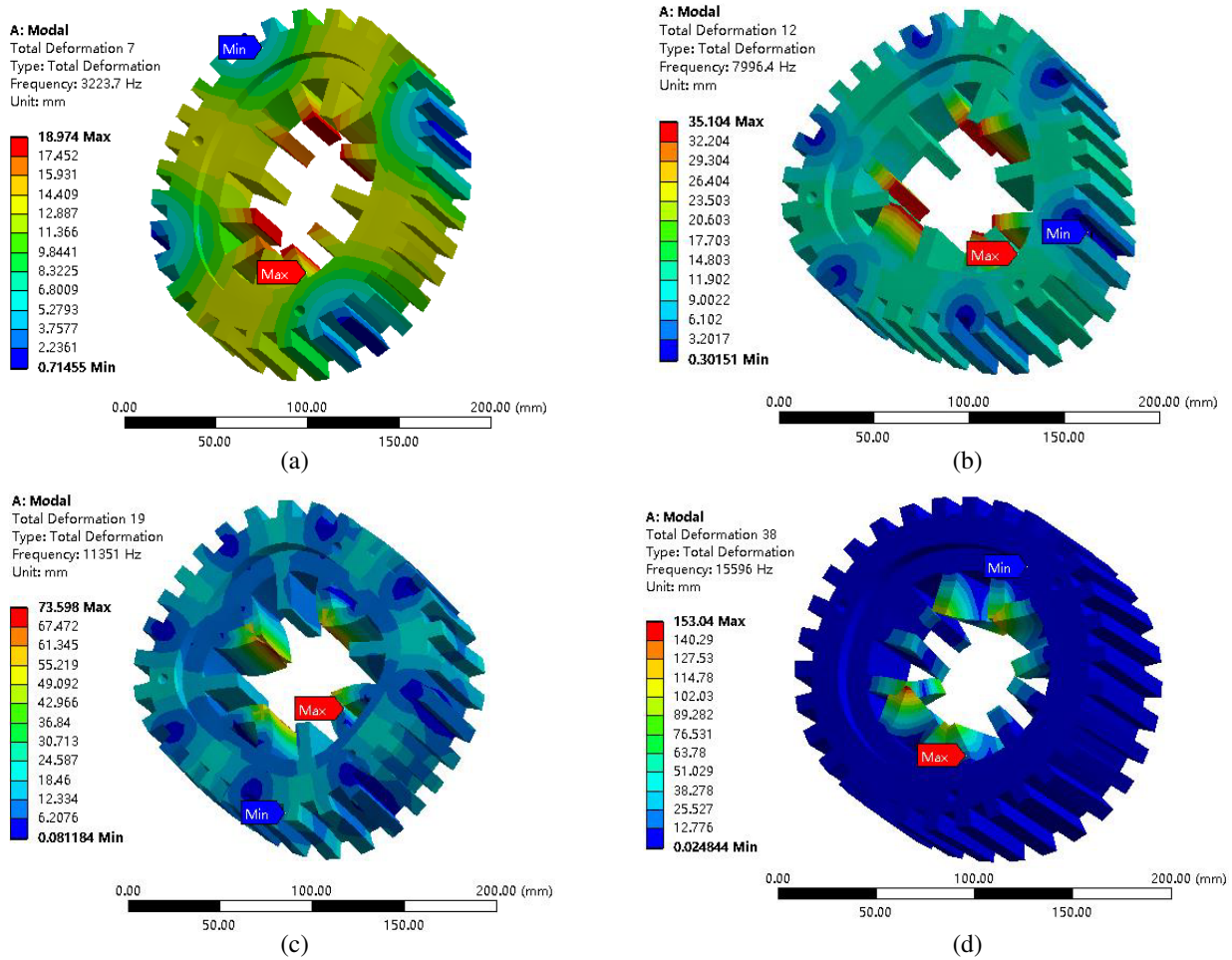


Figure 9. The basic mode shapes and frequencies ($m = 2, 3, 4, 5$) computation models of SWBSRM stator. (a) 3223.7 Hz, $m = 2$, (b) 7996.4 Hz, $m = 3$, (c) 11351 Hz, $m = 4$, (d) 15596 Hz, $m = 5$.

frequency range to 20 Hz–20 kHz which can be heard by the human ear. Fig. 9 shows the basic different modes shapes ($m = 2, 3, 4, 5$) computation models of SWBSRM stator.

From the simulation results of the 3D FEA of the SWBSRM stator, it can be seen that the vibration modes mainly include ellipse, triangle, quadrangle, and pentagon, which indicates that different shapes correspond to different frequencies. The red color of the stator tooth indicates that the force is relatively large, and the stator groove and yoke are blue-green, demonstrating that the force is relatively small. The natural frequency of the mode is close to the harmonic frequency of the radial electromagnetic force wave at 8000 Hz which is prone to resonance and thus causes large electromagnetic vibration. Through the modal analysis of the SWBSRM stator structure, it can effectively provide reference for motor design and optimization, to prevent the harmonic frequency of the radial electromagnetic force in SWBSRM from being consistent with the natural frequency of the motor during the design of the body, which will generate resonance and damage to the motor.

4. ANALYSIS OF ELECTROMAGNETIC VIBRATION AND NOISE CHARACTERISTICS

4.1. Analysis of Electromagnetic Vibration Characteristics

The electromagnetic vibration of SWBSRM involves the relationship between the electromagnetic field inside the motor and the structure field. It is necessary to consider the problem of the coupling between

the parameters of the two physical fields. According to the coupling mode of electromagnetic field and structure field inside the motor, the coupling analysis of motor vibration can be divided into magnetic-solid coupling and magnetic-solid weak coupling. Based on the research of the above two coupling modes combined with the purpose of this paper, the magnetic-solid weak coupling analysis method is adopted to analyze the electromagnetic vibration of the motor.

The vibration characteristics analysis of SWBSRM mainly considers the vibration response of the stator structure under the constraint of radial electromagnetic force. Therefore, it is necessary to suppress the torque component in actual operation. This paper uses ANSYS Workbench simulation software to introduce electromagnetic force into the harmonic response analysis field, and the radial electromagnetic force is loaded on the inner surface of the stator as shown in Fig. 10. Fig. 11 shows the vibration nephogram of the motor under the action of radial electromagnetic force.

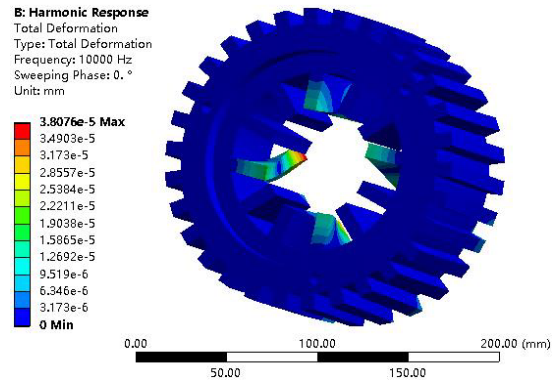
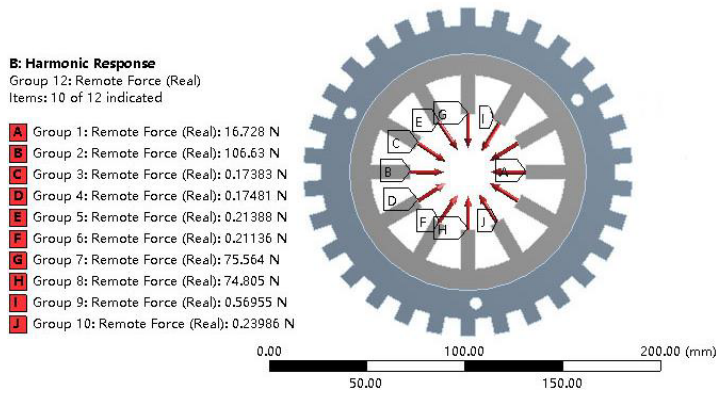


Figure 10. Radial electromagnetic force loading diagram.

Figure 11. Stator vibration nephogram.

It can be seen from the vibration nephogram that the vibration is generated by the electromagnetic force when the motor rotates causes the stator teeth to periodically deform. The force of the SWBSRM is mainly concentrated on the stator tooth portion, and the force on the stator tooth portion is significantly larger than that on the stator yoke portion and groove portion. Since the negative direction of the x -axis produces a larger radial electromagnetic force, a more pronounced deformation occurs here.

Under the excitation of radial electromagnetic force, the vibration acceleration waveform of the inner surface of the stator is obtained in the range of 0 Hz to 10000 Hz as shown in Fig. 12. It can be seen from the figure that the peak value of the vibration acceleration of the stator corresponds to the amplitude of the radial electromagnetic force, and the acceleration is also the extreme value at the extreme value of the amplitude when the acceleration extreme frequency is 8000 Hz. It is close to the third-order mode frequency which will lead to resonance, resulting in large vibration noise.

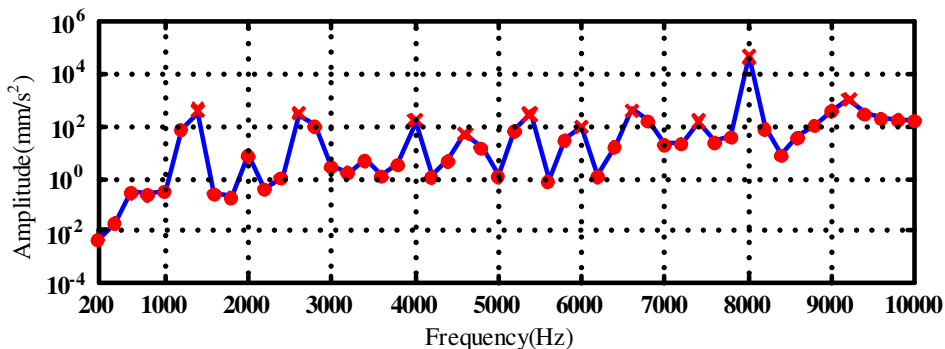


Figure 12. Vibration acceleration diagram.

4.2. Analysis of Electromagnetic Noise Characteristics

The research shows that the main reason for the electromagnetic noise of the motor is the vibration of the stator structure. When electromagnetic vibration occurs in SWBSRM, the amplitude and phase of vibration at various points on the outer surface of the motor will change with the change of frequency, and the vibration of the motor at different frequencies will change the distribution of sound pressure level of the motor. Therefore, in order to study the relationship between electromagnetic vibration and electromagnetic radiation sound pressure, it is necessary to establish a 3D structural model of motor sound pressure. This paper builds a sound pressure analysis model based on ANSYS Workbench finite element software. The noise is calculated by loading the speed of the motor surface node that has been calculated in Section 4.1 on the noise analysis model. Fig. 13 shows the motor noise analysis model, and Fig. 14 shows the local velocity loading model.

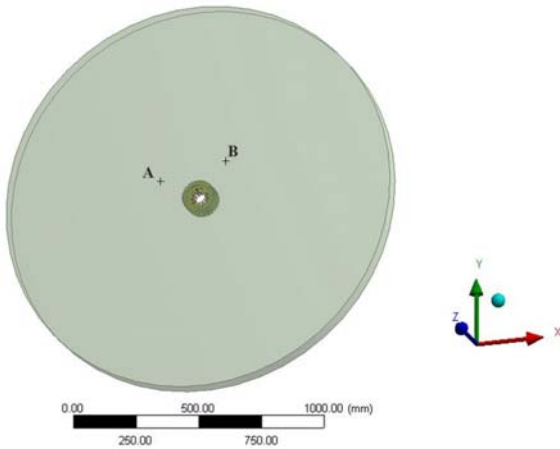


Figure 13. Noise analysis model.

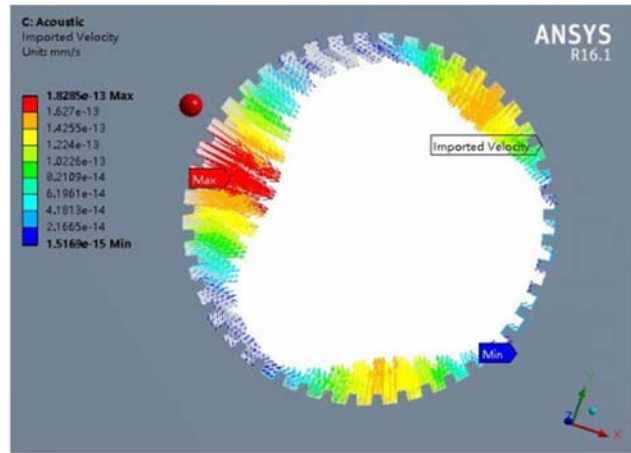


Figure 14. Local velocity loading model.

When the finite element method solves the motor sound field problem, its sound pressure satisfies the Helmholtz Equation (8):

$$\nabla^2 p + k'^2 p = 0 \tag{8}$$

$$k' = \omega / c \tag{9}$$

$$\nabla^2 p = \frac{\partial^2 p}{\partial x^2} + \frac{\partial^2 p}{\partial y^2} + \frac{\partial^2 p}{\partial z^2} \tag{10}$$

where p — sound field pressure; k' — wave number of sound waves; ω — frequency of sound waves; c — speed of sound; ∇^2 — Laplace differential operator.

Since the difference in the range of numerical changes of the sound pressure is too large, a reference amount is generally introduced, which is expressed in a logarithmic form, called a sound pressure level:

$$L_p = 20 \log \frac{p_r}{p_0} \tag{11}$$

where p_r is the sound pressure value to be tested; p_0 is the reference sound pressure, and $p_0 = 2 \times 10^{-5} / pa$

To calculate the sound pressure of SWBSRM, it is necessary to define the field point. Two output points of sound pressure value are set up in this paper and shown in Fig. 13 as points A and B, and Fig. 15 is the simulation result of the sound pressure level value of the field point. It can be seen that as the frequency increases, the sound pressure level of SWBSRM also shows an upward trend, and there is an extreme value at 8000 Hz where the noise is the largest.

Figure 16 shows nephograms of sound pressure values and sound pressure level values at the frequency of 8000 Hz. From the figure, it can be found that the noises radiated by SWBSRM at different field points are different, when the frequency is 8000 Hz, the electromagnetic force wave frequency is

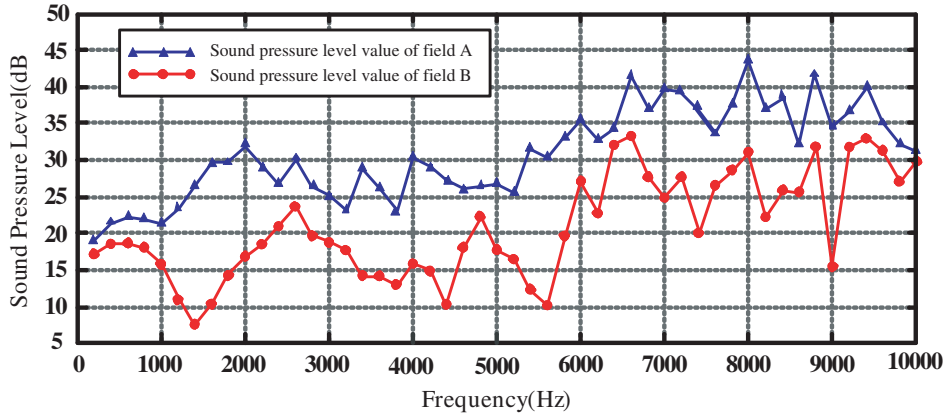


Figure 15. Sound pressure level value of the output field.

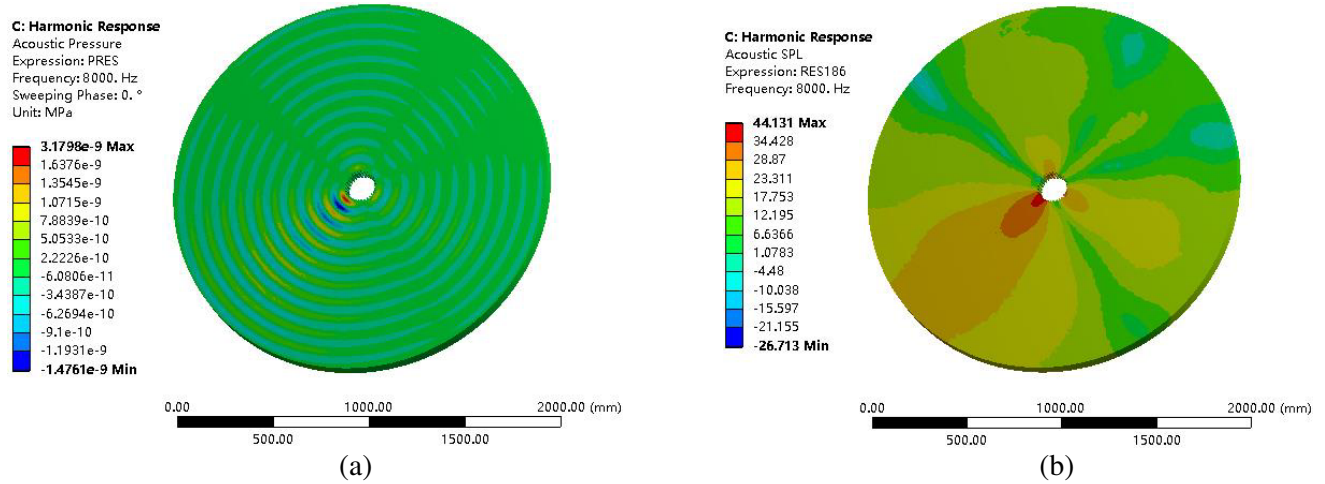


Figure 16. Sound pressure nephogram at 8000 Hz. (a) Acoustic pressure nephogram. (b) Acoustic SPL nephogram.

consistent with the natural frequency of the motor. At this time, resonance occurs, and the noise is the largest. The maximum value is 44.131 dB.

5. CONCLUSION

In this paper, a complete model of electromagnetic field, structural vibration, and noise radiation is established for the main causes of SWBSRM electromagnetic vibration and noise. The magnetic flux density in the air gap and the amplitude and frequency of the radial electromagnetic force wave are analyzed, and then the modal analysis of the stator structure is carried out, and its natural frequency and mode shape are obtained. Through harmonic response analysis and sound pressure analysis, the vibration response of the motor and noise sound pressure radiated therefrom are obtained. According to the simulation results, it can be concluded that when the radial electromagnetic force is large, the vibration deformation and noise are also relatively large. When the electromagnetic force wave frequency and inherent frequency of the motor are identical, the resonance occurs, and the noise is the largest at this time. In summary, the results of electromagnetic vibration and noise analysis are consistent with the previous estimates. The results show that the established model and analysis method are correct and feasible. The same method can be used to deal with other types of motors, which has certain guiding significance for motor optimization design and prediction of motor vibration and noise.

ACKNOWLEDGMENT

This work was supported in part by the National Natural Science Foundation of China under Project 51707082 and Project 51877101, by Natural Science Foundation of Jiangsu Province of China (Grants No. BK20170546, No. BK20150510), and by the Priority Academic Program Development of Jiangsu Higher Education Institutions (PAPD).

REFERENCES

1. Liaw, C. M., K. W. Hu, J. C. Wang, et al., "Development and operation control of a switched-reluctance motor driven flywheel," *IEEE Transactions on Power Electronics*, Vol. 34, No. 1, 526–537, 2018.
2. Takemoto, M., A. Chiba, H. Akagi, et al., "Radial force and torque of a bearingless switched reluctance motor operating in a region of magnetic saturation," *IEEE Transactions on Industry Applications*, Vol. 1, No. 1, 103–112, 2002.
3. Yuan, Y., Y. Sun, and Y. Huang, "Design and analysis of bearingless flywheel motor specially for flywheel energy storage," *Electronics Letters*, Vol. 52, No. 1, 66–68, 2015.
4. Wu, C. Y. and C. Pollock, "Time domain analysis of vibration and acoustic noise in the switched reluctance drive," *IEE Sixth International Conference on Electrical Machines and Drives*, 558–563, London, UK, 1993.
5. Callegaro, A. D., J. Liang, J. W. Jiang, et al., "Radial force density analysis of switched reluctance machines: The source of acoustic noise," *IEEE Transactions on Transportation Electrification*, Vol. 5, No. 1, 93–106, 2018.
6. Sun, J., Q. Zhan, S. Wang, et al., "A novel radiating rib structure in switched reluctance motors for low acoustic noise," *IEEE Transactions on Magnetics*, Vol. 43, No. 9, 3630–3637, 2007.
7. Sun, J. B., "A novel control strategy of switched reluctance motor contributing to low vibrative noise and minimal torque ripple," *Proceedings of the Csee*, Vol. 28, No. 12, 134–138, 2008.
8. Li, J., X. Song, and Y. Cho, "Comparison of 12/8 and 6/4 switched reluctance motor: Noise and vibration aspects," *IEEE Transactions on Magnetics*, Vol. 44, No. 11, 4131–4134, 2008.
9. Zhang, J. J., R. Long, H. J. Zhang, et al., "Analytical and FEM modeling of electromagnetic radial force for switched reluctance motor," *Applied Mechanics and Materials*, 121–126, No. 4, 3765–3769, 2011.
10. Sun, J. B., Q. H. Zhan, and J. Huang, "Modal analysis of stator vibration for switched reluctance motors," *Proceedings of the Csee*, Vol. 25, No. 22, 148–152, 2005.
11. Guo, X., R. Zhong, M. Zhang, et al., "Fast computation of radial vibration in switched reluctance motors," *IEEE Transactions on Industrial Electronics*, Vol. 65, No. 6, 4588–4598, 2017.
12. Anwar, M. N. and I. Husain, "Radial force calculation and acoustic noise prediction in switched reluctance machines," *IEEE Trans Industry Applications*, Vol. 36, No. 6, 1589–1597, 2000.
13. Yang, H. Y., Y. C. Lim, and H. C. Kim, "Acoustic noise/vibration reduction of a single-phase SRM using skewed stator and rotor," *IEEE Transactions on Industrial Electronics*, Vol. 60, No. 10, 4292–4300, 2013.
14. Castano, S. M., B. Bilgin, J. Lin, et al., "Radial forces and vibration analysis in an external-rotor switched reluctance machine," *IET Electric Power Applications*, Vol. 11, No. 2, 252–259, 2017.
15. Yang, Y., Z. Deng, X. Cao, et al., "Characteristic analysis of stator vibration for 12/8 bearingless switched reluctance motors," *Journal of Nanjing University of Aeronautics & Astronautics*, Vol. 42, No. 4, 494–500, 2010.
16. Wang, X., Q. Tan, X. Liu, et al., "Improved radial force modeling and rotor suspension dynamics simulation studies for double-winding bearingless switched reluctance motor," *Electric Power Components and Systems*, Vol. 45, No. 1, 111–120, 2017.
17. Takemoto, M., A. Chiba, H. Akagi, et al., "Radial force and torque of a bearingless switched reluctance motor operating in a region of magnetic saturation," *IEEE Transactions on Industry Applications*, Vol. 1, No. 1, 103–112, 2004.

18. Yang, G., Z. Deng, X. Cao, et al., "Optimal winding arrangements of a bearingless switched reluctance motor," *IEEE Transactions on Power Electronics*, Vol. 23, No. 6, 3056–3066, 2008.
19. Chen, L. and W. Hofmann, "Speed regulation technique of one bearingless 8/6 switched reluctance motor with simpler single winding structure," *IEEE Transactions on Industrial Electronics*, Vol. 59, No. 6, 2592–2600, 2012.
20. Yuan, Y., Y. Sun, and Y. Huang, "Radial force dynamic current compensation method of single winding bearingless flywheel motor," *IET Power Electronics*, Vol. 8, No. 7, 1224–1229, 2015.